A Colorimetric Humidity Sensor Based on Liquid Composite Materials for the Monitoring of Food and Pharmaceuticals.

Devon Bridgeman[†‡], Javier Corral[‡], Ashley Quach[†], Xiaojun Xian[†], and Erica Forzani[†‡*]*

[†]Center for Bioelectronics and Biosensors, Biodesign Institute, Arizona State University.

[‡]Fulton School of Engineering Matter, Transport, and Energy.

ABSTRACT

Using supported ionic-liquid membrane (SILM)-inspired methodologies, we have synthesized, characterized, and developed a humidity sensor by coating a liquid composite material on a hygroscopic and porous substrate. Similar to pH paper, the sensor responds to the environment's relative humidity and changes color accordingly. The humidity indicator is prepared by casting few microliters of low toxicity reagents on a non-toxic substrate. The sensing material is a newly synthesized liquid composite, which comprises a hygroscopic medium for environmental humidity capture, and a color indicator, which translates the humidity level into a distinct color change. Sodium borohydride was used to form a liquid composite medium and DenimBlu30 dye was used as a redox indicator. The liquid composite medium provides a hygroscopic response to relative humidity, and DenimBlu30 translates the chemical changes into a visual change from a

yellow to blue color. The borate-redox dye based humidity sensor was prepared, then Fourier Transform Infrared Spectroscopy, Differential Scanning Calorimetry, and image analysis methods were used to characterize chemical composition, optimize synthesis, and gain insight into sensor reactivity. Test results indicated that this new sensing material can detect relative humidity in the range of 5-100% in an irreversible manner with good reproducibility and high accuracy. The sensor is a low cost, highly sensitive, and easy-to-use humidity indicator. More importantly, it can be easily packaged with products to monitor humidity levels in pharmaceutical and food packaging.

INTRODUCTION

Many products, ranging from food and pharmaceuticals to semiconductors and natural gas, face issues with product degradation in the presence of humidity[1-4]. In many cases, product damage due to the effect of humidity is difficult to assess before use. In pharmaceuticals, for example, humidity can cause issues with degradation of active ingredients resulting in decreased effects or changes in the auto adhesive properties of drugs, resulting in deviations from expected delivery times[3]. Most of the time, pharmaceutical products need to be stable within the 25% - 75% range of relative humidity; food products need a constant humidity range depending on the application[1-3]. Humidity monitoring of consumer products requires an inexpensive, simple, and equipment-free sensor with a relatively low toxicity.

In semiconductor packaging, desiccant evaluation, and similar measurements humidity monitoring is needed on a large scale, but at a low cost. Cobalt (II) chloride is commonly used for these applications, but it is unsuited for purposes where irreversibility is required and toxicity is a concern[5-6]. Other metal chlorides have been proposed and produced, but unfortunately they are still somewhat toxic and have a much higher cost than cobalt (II) chloride[7]. Moreover, metal

chloride based humidity sensors can also cause environmental damage when disposed. Photonic crystal sensors have gathered a large amount of attention as a low cost optical humidity sensor due to their highly sensitive visual response to changes in humidity, but unfortunately most cannot accurately detect low levels of humidity and are intrinsically reversible sensors[8-11]. A highly sensitive, irreversible, environmentally friendly, and low-cost humidity indicator, therefore, is needed for humidity monitoring of common consumer goods.

In this paper, we describe the characteristics and developmental details of a new type of colorimetric humidity sensor based on a liquid composite material. The sensing material used for sensing consists mainly of a viscous medium that provides hygroscopic characteristics for environmental humidity capture, and a redox indicator that translates the humidity level of the matrix into a distinct color change. DenimBlu30, which has been previously used for detection of oxygen in aqueous solutions, is used as the redox indicator[12-13]. DeminBlu30 is yellow in its reduced form and turns blue upon oxidation. The choice of DenimBlu30 is strategic because it has been approved for use as a food colorant in the United States and the EU and is currently considered safe for use in many end consumer products, including blue jeans and food[14-15].

The new colorimetric sensor described here has several advantages over conventional instruments. First, the sensor is comprised of well-known compounds of low toxicity, making it much safer than cobalt (II) chloride sensors for humidity monitoring of pharmaceutical or food products[16-20]. Second, the preparation of the material for the sensor utilizes relatively mild chemicals and consists of a very simple process. Third, it was found that the probe material and matrix do not readily degrade under standard conditions when unreacted and kept dry[21-23]. Finally, the sensing material was found to easily detect peak humidity levels in the range 5-100%

relative humidity, providing a sensor that can be very easily mass produced and has potential applications in pharmaceutical and food packaging.

EXPERIMENTAL

Materials

DenimBlu30 (high purity, biological stain), ethanol (200 proof, analytical grade), potassium acetate (99%), magnesium chloride hexahydrate, and silica gel were purchased from Sigma-Aldrich. Sodium hydroxide (99.3%) was purchased from Fisher Scientific, and sodium borohydride (98%) was purchased from EMD Millipore. Water (18 MΩ.cm) was purified using an ELGA Purelab Ultra reverse osmosis water purifier.

Sensing Solution and Sensor Preparation

Sensing solution preparation: Solutions consisted of sodium borohydride, sodium hydroxide (pH ~10), water (10ml), Denimblu30 (saturation), and ethanol (3.75ml) mixed and purged with ultra-high purity nitrogen. After mixing, they were transferred to a nitrogen environment glove box (VAC OMNI-LAB) for storage and casting.

Sensor preparation: Sensors were prepared using GENETIX polypropylene 384-well plates as substrates. Firstly, unmodified silica gel with gypsum (60 Å porosity, 5-15µm particle size, 500-600 m^2/g surface area) was cast in individual wells of the plate and dried in ambient conditions. Plates were then transferred to a glove box and the sensing solution (13µl/well) was added to the wells. Well plates were then allowed to dry for 2 days before testing. The well plates were used only to control the drying rate of the coated silica gel; the silica gel was tested in the well plates for simplicity.

Glove Box Conditions

Samples were prepared under inert atmosphere conditions in a VAC OMNI-LAB glove box with ultra-high purity nitrogen. Humidity levels typically remained at 0.5 ppm (0.002% RH) with peak levels of 10 ppm, and oxygen levels typically remained at 0.1 ppm with peaks of less than 1 ppm. After the appropriate amount of aging time, samples were cast and allowed to dry.

Fourier Transform Infrared Spectroscopy (FTIR) Measurements

All FTIR measurements were taken using a Thermo-Scientific Nicolet 7600 FTIR spectrometer equipped with a Smart Orbit diamond plate single reflectance ATR unit. Samples for FTIR analysis were prepared by casting 50 uL samples on glass slides in glove box conditions, and then scanned via diamond ATR crystal. Background spectrums were averaged over 64 scans and sample spectrums were averaged over 32 scans. Samples were measured with a resolution of ~2 cm^{-1} in the range of 500 cm^{-1} to 4000 cm^{-1}.

Differential Scanning Calorimetry (DSC) Measurements

DSC measurements were performed using a Thermal Advantage DSC and -40 °C refrigerated cooling system with ultra-high purity nitrogen gas flow. Samples were prepared in aluminum hermetic DSC pans in masses ranging from ~3mg - ~5mg. Sample pans were loaded and pressed under inert conditions in a MBRAUN Labmaster 130 glove box. DSC samples were prepared by casting 50 uL samples of solution on glass slides, then transferring the dried sensing material to a hermetic aluminum DSC pan. An empty hermetic pan was used as a reference and a ramp rate of 10 $^{\circ}$C/min was used for all tests. The same reference pan was used for all experiments.

Humidity detection and calibration

Intensity measurements were taken using a Logitech webcam in a closed container with saturated salt solutions for humidity measurement. Ambient conditions of saturated potassium acetate (~23% RH), saturated magnesium chloride (~33% RH), saturated sodium chloride (~75% RH), and water (~100% RH) were used as calibration humidity controls. Two hours were allowed for equilibration of sensors in a close environment with a humidity control solution, and then images of the sensors were taken and processed. RGB Image processing was done in ImageJ (NIH) by taking the signal as the blue or red intensity normalized by the grey intensity (sum of the intensity of all components), which provided maximum sensitivity to humidity.

RESULTS AND DISCUSSION

Fourier Transform Infrared Spectroscopy Study

As explained in the sensor preparation subsection of the experimental section, once the sensing material's components were combined, they were stored in an inert ultra-low humidity environment (glove box) at room temperature. Spontaneous reaction of the solution occurring under inert conditions determined the final sensing mixture composition, with time being the main factor. Fourier Transform Infrared Spectroscopy (FTIR) was employed to evaluate the optimized aging time of the final sensing mixture. In addition, Differential Scanning Calorimetry (DSC) was used to evaluate thermal transitions of the sensing mixture with heat exposure (see below). Preparation conditions of the sensing mixture, used as a sensing material, were optimized, allowing for a chemically and thermally stable sensor.

It is worth noting that the sensing material was prepared by aging the solution of sodium borohydrate and the redox indicator in an alkaline media in the absence of oxygen and humidity (see reaction mechanism section), the pH of which ranged from ~7.5 to ~9. Figures 1A and 2 show FTIR spectra by which changes in chemical moieties of the sensing solution can be observed over the course of the solution aging process. Peaks due to vibrations, symmetric stretching, and asymmetric stretching of water typically occurring at 1885 cm^{-1}, 3506 cm^{-1}, and 3685 cm^{-1}, were observed for this sensing at ~1625 cm^{-1}, ~3450 cm^{-1}, and ~3550 cm^{-1}, which gives insight into changes in the sensing material's bonding environment[24]. This specific type of shift has been reported to be characteristic of very polar bonding environments in aqueous systems[25-26]. In addition, Figure 1A shows that the characteristic peaks of sodium borohydride diminished at 1105 cm^{-1}, 2220 cm^{-1}, and 2275 cm^{-1}, and new peaks appeared between 1800 cm^{-1} – 2300 cm^{-1}, indicating the presence of the hydrogen-bridged boron structures of diborane[27-31]. Additionally, a strong peak increasing in intensity at ~ 850 cm^{-1} indicated an increase in the concentration of orthoborates, which are expected during the aging of sodium borohydride[31]. It is worth noticing that main changes of chemical moieties occurred during the first 3 days of aging.

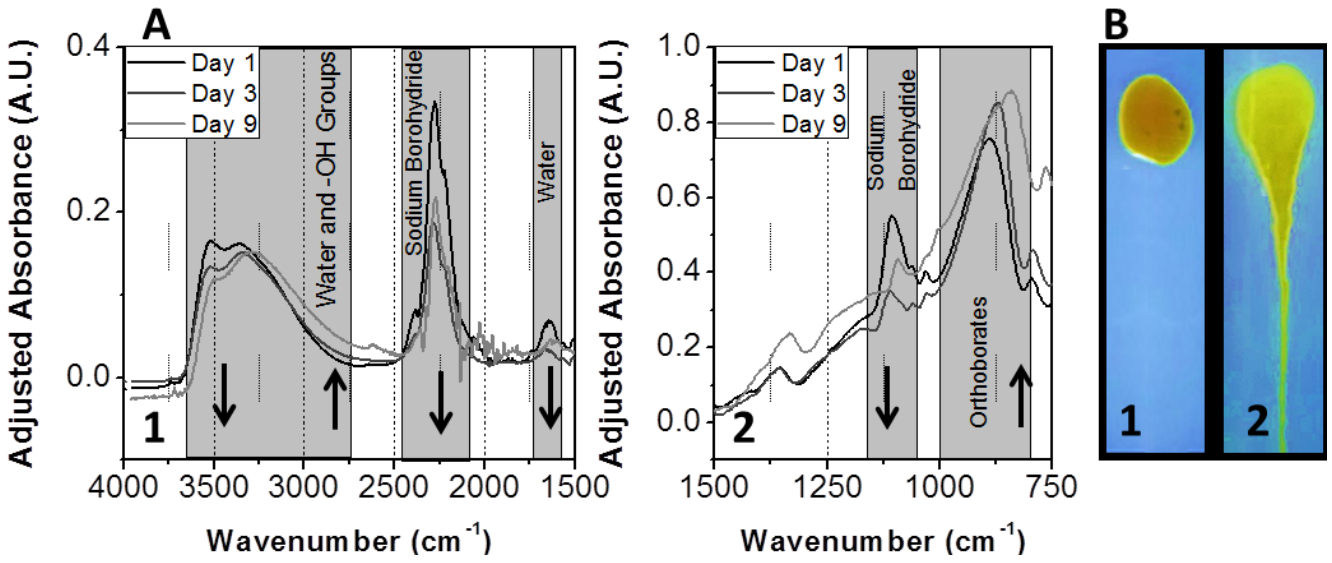

Figure 1. (A) FTIR spectra of sensing materials cast and dried after different days of aging in a glove box environment, short and mid IR regions. (B) Cast and dried sensing material before (1) and after (2) centrifugation. The test was performed to demonstrate the liquid nature of the sensing material at room temperature.

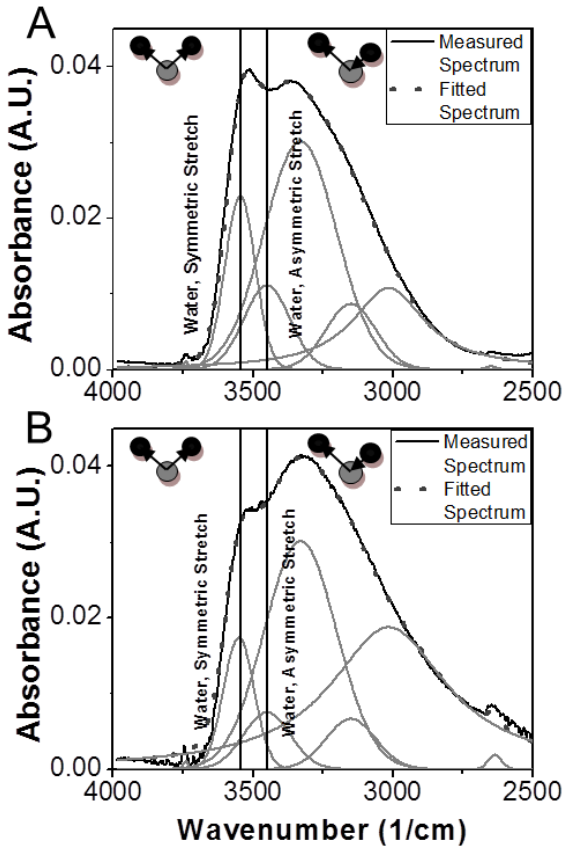

Figure 2. FTIR spectra from non-aged (A) and 9-day aged (B) sensing solution. Grey lines represent unmixed simulated curves. The black line represents experimental spectra.

In order to characterize the water shift phenomena, spectral unmixing simulation of the above-mentioned water and –OH peaks was performed by fitting gaussian and lorentzian distributions to the spectrum until the sum of all distributions produced a peak that matched the experimental

peak with a good fit. Figure 2 shows the experimental and unmixed simulated spectra, and it can be seen that the peak at ~3300 cm^{-1} can be separated into several secondary peaks corresponding to water and other -OH containing compounds. Since during the course of the reaction orthoborate concentrations rise (at ~850 cm^{-1}), -OH containing groups were attributed to said borate species and considered to be responsible for the changes in bonding environment arising from the aging process. Increases in pH of the solution from about 7.5 to 9 were measured in the course of sensing material aging (from day 1 to day 9), which is in agreement with the formation of polyborates during the course of aging[29]. Distribution of borates species (mainly $B(OH)_3$, $B_5O_6(OH)_4^-$, $B_3O_3(OH)_4^-$, $B_4O_5(OH)_4^{2-}$,$B_3O_3(OH)_5^{2-}$,and $B(OH)_4^-$) is highly dependent on temperature, pH, counter-ion, and concentration. The observed change in pH is indicative of a change in the distribution of equilibrium concentrations in the borate mixture[28-30, 32].

It is important to note that the aging of the sensing solution not only brings chemical changes, but also significant changes in physical properties. The cast and thoroughly dried sensing material turns into a highly viscous liquid with aging, which can be easily dispersed by the action of centrifugation (Figure 1 B).

. We consider the material to be a liquid composite, since it is a liquid by virtue of its diverse composition, being composed of very little solvent (see DSC analysis below) and mostly species that are highly crystalline under the same conditions when pure. Additionally, gravimetric measurements showed that the dried solution only weighed roughly 40% more than the total amount of solids added initially (after 9 days of aging). Since it is well known that much of the water is incorporated into the borate products (see below), this reinforces the notion that very little of the final sensing element is free water.[33-35]

Solution aging was a key point for the liquid composite medium formation; it was found that a chemically stable product resulted from 9 or more days of aging.

Differential Scanning Calorimetry (DSC)

DSC was performed to evaluate the thermal properties and thermal stability of the non-aged and aged sensing material. Figure 3A shows DSC scans for sensing material samples aged for 1, 4, 9, and 14 days. In addition, the heat absorbed (lower portion of the scan) and released (top portion of the scan) during the scan was evaluated during heating and cooling (Figure 3B). Likewise, heating and cooling glass transition temperatures were extracted. In all samples, heating glass transitions were observed from -12 °C to 35 °C and a small degree of quenching and annealing was seen during cooling at -15 °C [36]. From Figure 3B, it can be observed that the sensing material's heat capacity decreased and approached constant values as aging time increased. This is consistent with a drop in water content, as water has roughly double the heat capacity of anticipated borate products [37].

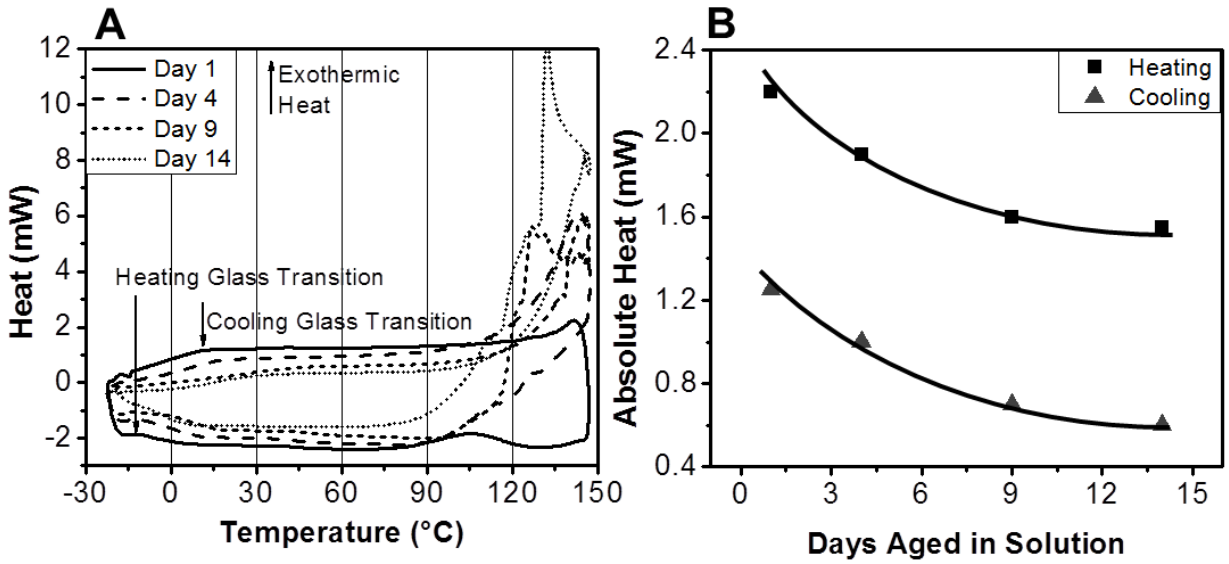

Figure 3. (A) DSC curves for samples aged different times in aqueous media. (B) Heat capacity of sensing material vs. aging time of the solution used as sensing material. Note: absolute values are not corrected, and they may include instrument offset. However, testing offset is equal for each test.

It is worth noting in Figure 3A that higher values of heat, indicating an exothermic process, were released once the samples were exposed to temperatures higher than 90 °C. In addition, the degree of the exothermic process was elevated for longer aged sensing samples. This exothermic reaction may occur due to the presence of borate products in aged samples. It is hypothesized that some borate products (e.g., diborane) could react with the aluminum capsule used for testing. This exothermic reaction, in addition to glass transition temperatures (see below), were utilized to access the stability of the synthesized sensing material over time.

In order to stabilize the aged sensing material, a heat treatment at 50^{o}C was applied. Aged sensing samples treated at 50 °C did not show destructive exothermic behavior after (at least) 1 week of treatment. Figure 4A shows an example of DSC scans for 9-day aged sensing samples untreated, and then treated with heat for 1, 2, and 6 weeks. In all heated samples, destructive exothermic behavior was not observed below 100 °C during high temperature DSC tests. In addition, the stability gained for heat treatment was found to be permanent. This effect is demonstrated in Figure 4B.

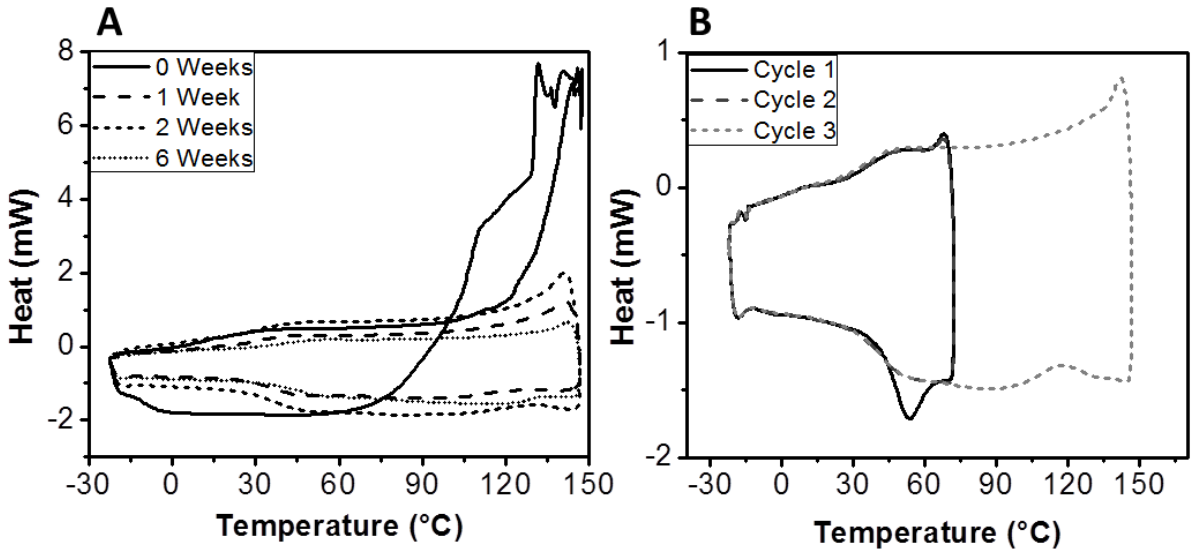

Figure 4. (A) DSC curves of sensing materials cycled from -20 to 150 °C after 2 cycles from -20-75 °C. The sensing materials were left at 50 °C for different times. (B) DSC curve of sensing material at low (up to 70°C for 1st and 2nd cycles), and at high (150°C for 3rd cycle) temperatures. The sensing material sample was previously treated with heat at 50 °C for 5 weeks and left at 25 °C for 1 week.

During the course of this work, DSC thermal cycling was performed and the analysis of changes between cycles was noted to be indicative of thermal stability. As evidenced by cooling glass transition temperatures shown in Figure 5A, the temperature of the first cooling glass transition shifted notably in non-aged solution samples during thermal cycling. The shift became more evident with sensing samples that were further aged. However, the shift disappeared for heat-treated aged sensing samples. The stability shown in the glass transition temperature after heating (Fig. 5A) was also observed in heat-treated sample kept at room temperature (not shown). This is in agreement with the stability gained in the inhibition of the exothermic process

(discussed above). Therefore, it can be concluded that oven aging of the sensing samples results in thermal stability gains that are retained over time at room temperature conditions.

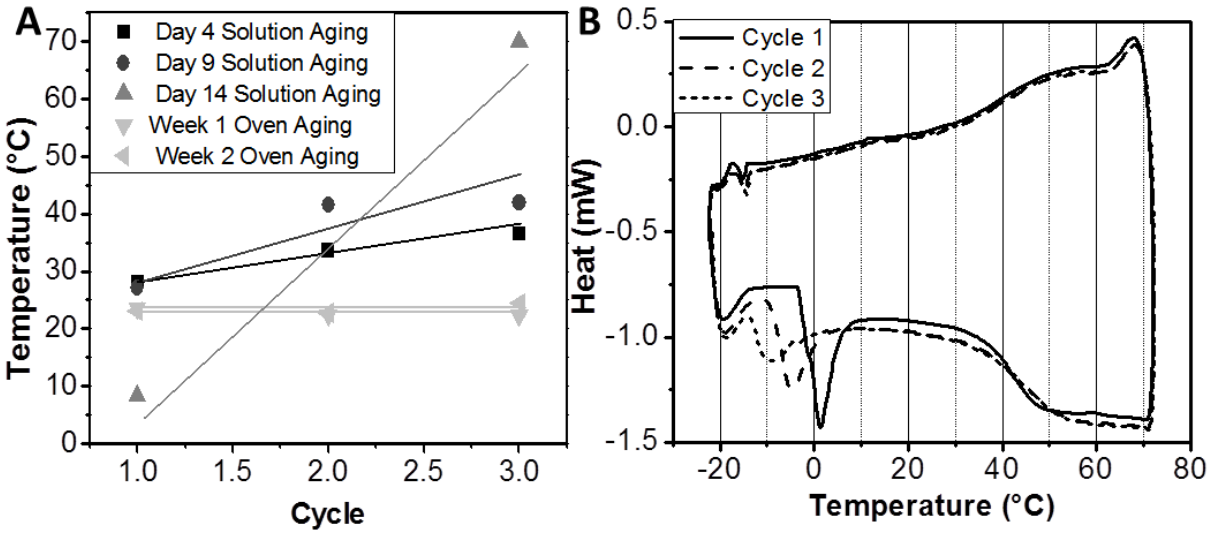

Figure 5. (A) Cooling glass transition temperature vs. cycle number, with first 2 cycles ramping from -20 to 75 °C, then the third cycle ramping from -20 to 150 °C for different aged sensing material samples (4, 9, and 14 days), and 14-day aged sensing samples treated with heat at 50°C (1 and 2 week oven aging). (B) DSC curve from thermal cycling of a slightly hydrated sample (see text for details).

An investigation of hydrated samples provides further evidence of the low-solvent nature of the liquid composite. It is well known that weakly associating water in the sensing material can be detected by a melting point at slightly below 0°C[36]. In Figure 5B, a sample that had not dried to the same degree as the rest of the samples was cycled. It can be seen that the first cycle exhibits a melting point slightly below zero. In subsequent cycles, the melting point lowers in temperature, the melting peak broadens, and the melting peak lowers in intensity. This is

indicative of water in the borate matrix that is weakly associating with the chemical environment; this free water begins to associate more strongly with the matrix on each thermal cycle. The lack of this feature in the remaining DSC curves indicates that little to no free water is present in the sensor. Thermal cycling demonstrated that increases in instability from solution aging could be alleviated by oven aging of the prepared sensor. This reinforces the notion that our sensing material is a liquid composite material with little to no characteristics of free water.

Humidity Detection

As described in the experimental section, the sensing material was deposited onto silica substrate. Optical measurements were taken with sensor exposure to different humidity levels. Figure 6A shows the absorbance spectra of the sensing material before and after the exposure to humidity. It can be observed that the wavelengths corresponding to Blue and Red RGB components were the most affected by the humidity-induced color change. The Blue and Red intensity changes were normalized by the sum of the intensity of all components (RGB), giving a measure of chromaticity change, and studied as a function of relative humidity levels. Figure 6B summarizes the most relevant results of the system. It is worth noticing that the normalized Red signal gave out greater sensitivity at low relative humidity levels, while the normalized blue signal showed greater sensitivity at high relative humidity levels.

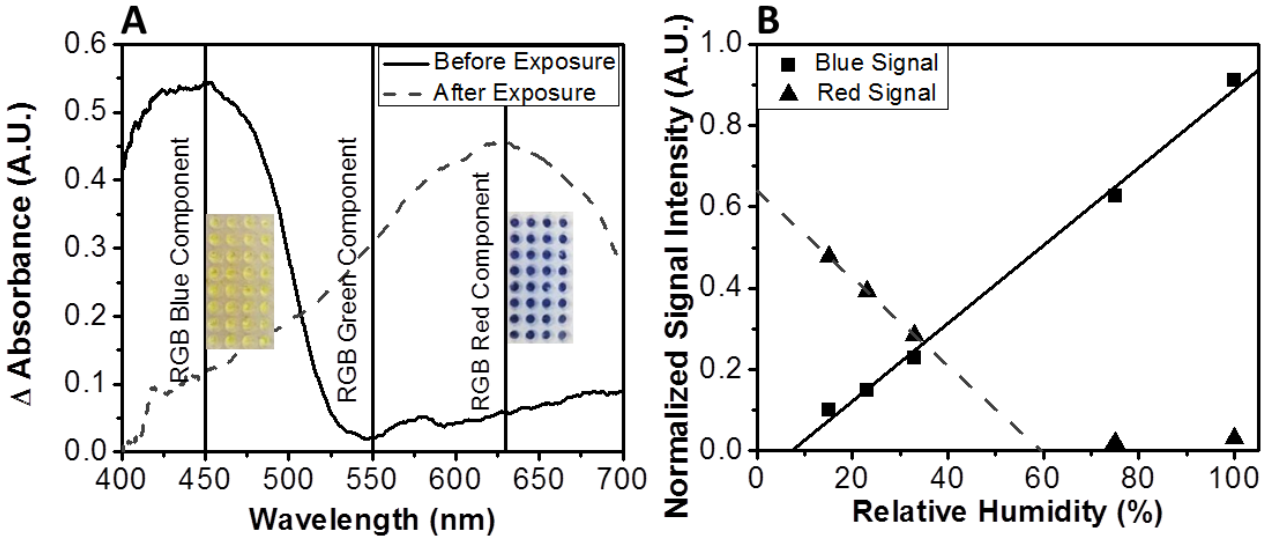

Figure 6. (A) Absorbance spectra of sensing material. The changes are due to reduced and oxidized dye. RGB wavelengths are marked with solid vertical lines, along with pictures of the new humidity sensor. (B) Calibration curve of the new humidity sensor. Relationship between the new humidity sensor signal and relative humidity assessed with a reference humidity sensing device. The sensor signals were taken as the intensity (red or blue) change over the total intensity (red + blue + green) of the sensor.

Another interesting feature observed was that when placed in a dry environment after two or more hours of equilibration to a set humidity, the sensors did not display reversible behavior. This is likely due to the high stability of the reduced form of the redox dye in this medium. Figure 7 shows comparative results assessed between the new calibrated colorimetric humidity sensors and either ambient relative humidity levels measured via hygrometer or humidity controlled by saturated salt solution. It can be observed that calibration of the sensor using a CMOS chip from a webcam setup illuminated by ambient lighting can provide relatively accurate results that are in good agreement with the reference sensor, with errors not exceeding

12%. Overall, we found the sensor capable of detecting humidity levels with a standard deviation of roughly 3.3% relative humidity, which could be improved upon by better preparation methods, testing conditions, and signal processing. The sensing reaction takes between 50-70 minutes to equilibrate under natural diffusion. It is worth noting that~~,~~ the sensor response may be accelerated by using different sensor configuration and forced convective. Despite improvements being needed, our sensor still provides improved resolution than the typical cobalt (II) chloride sensor without utilizing toxic materials.

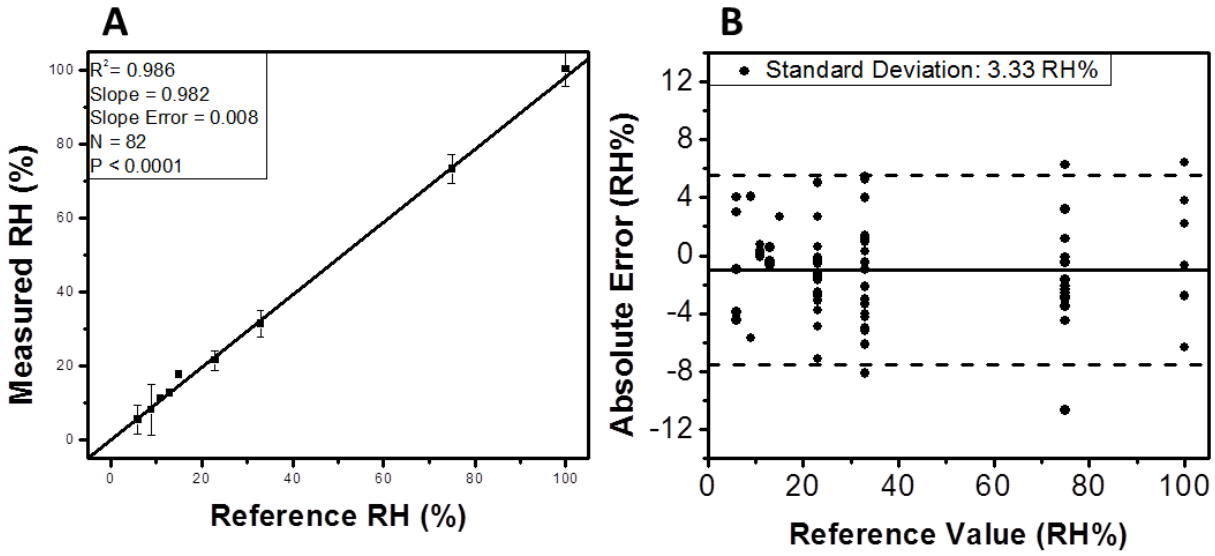

Figure 7. (A) The relationship of relative humidity readings (RH %) between the new humidity sensor and a reference humidity sensing device. (B) Bland-Altman plot comparing the new sensor's absolute errors to the reference humidity sensing device in a range from 0 to 100% with dotted lines representing the 95% confidence limits.

Reaction Mechanism

The borate matrix is produced in aqueous conditions by the reaction of sodium borohydride with water, producing mainly $NaBO_2$ by the irreversible reaction: [28-30, 32-33, 35]

$NaBH_4(aq) + 2H_2O(l) \rightarrow NaBO_2(aq) + 4H_2(g)$

The reaction product, $NaBO_2$, is hydrated to generate $NaB(OH)_4$, which then equilibrates reversibly into a diverse mixture of borate ions. In simple aqueous systems, borate ion solutions can contain over a dozen components, since the composition depends on temperature, pH, concentration of species, and counter-ions[28-30, 32]. The aqueous borate solution is then coated on silica gel and dehydrated. This sensing material product maintains itself as a liquid composite coating providing a very strong hydrogen bonding environment, as discussed above.

While in the dehydrated state, the strong hydrogen bonding environment does not allow oxidation of the redox dye, despite ambient conditions holding ample oxygen (generally 20.5%). This is possibly due to unfavorable reaction environment and/or extremely low permeability of the liquid composite coating to oxygen. Humidity detection is attained by embedding this redox dye in the borate matrix and taking advantage of its strong hydrogen bonding borate environment, which is favorable for water absorption. Once the dye-modified liquid-composite material is exposed to water, absorption of water induces an improvement of dye-oxygen reaction environment and/or increase in the liquid composite's affinity for oxygen, resulting in a visual oxidation of the redox dye from yellow to blue[38], which is made irreversible ~~if the~~by the liquid-composite being deposited on silica; the liquid composite itself has shown reversibility when ~~is~~ exposed ~~back~~ to a dry environment after reaction. It is also worth remarking that the sensor is designed and tested for ambient oxygen levels (20.5%).

In addition, it was found that by varying the film thickness of the sensing liquid composite on the silica gel the sensitivity and dynamic range of the sensor can be easily tuned. Thick coating sensing films were more sensitive to higher humidity levels, while thinner coating

sensing films were more sensitive to lower humidity levels. This is an interesting feature for implementation of the sensor in real sensing conditions and broad humidity level range.

Stability

The sensing material developed herein has shown great long-term stability in room temperature settings. Sensors that have been exposed to dry environments with high and low oxygen concentration have shown no signs of visual color changes or degradation of the material for over 4, and 12 months, respectively.

CONCLUSION

The borate-redox dye based humidity sensor was successfully prepared, and systematic characterizations were performed using FTIR, DSC, and imaging methods to gain insight into the composition, sensor stability, and reactivity. The extent of reaction of sodium borohyride in the sensing solution was monitored via FTIR, and showed that after 9 days of solution aging a chemically stable liquid composite sensing material could be produced. By DSC screening, we found that further aging in the dried state at elevated temperature produced a thermally stable sensing material. By aging the dried sensor at 50 °C, thermal stability could be established as per evaluation by traditional and cyclic DSC methods. The material was found to be stable over time in conditions similar to or more extreme than the needs of the food and pharmaceutical industries with the use of materials of low toxicity. The sensor can detect a relative humidity in the range of 5-100% in an irreversible manner with good reproducibility and high accuracy. This low-cost, highly sensitive, and easy-to-use humidity sensor can be sized to a miniaturized strip,

which makes it easy to be applied to product humidity monitoring in pharmaceutical or food products.

ABBREVIATIONS: SILM: Supported Ionic-Liquid Membrane, EU: European Union, FTIR: Fourier Transform Infrared Spectroscopy, ATR: Attenuated Total Reflectance, RH: Relative Humidity, DSC: Differential Scanning Calorimetry, ppm: Parts per Million (By Volume).

ACKNOWLEDGEMENT: We gratefully acknowledge the resources made available by the Fulton School of Engineering Matter, Transport, and Energy, and by Dr. NJ Tao though the Center of Bioelectronics and Biosensors, along with use of facilities within the LeRoy Eyring Center for Solid State Science at Arizona State University.

REFERENCES:

1. Rizvi, S. S. H.; Perdue, R. R. Requirements for foods packaged in polymeric films. *C R C Critical Reviews in Food Science and Nutrition* **1981,** *14* (2), 111.
2. Yam, K. L.; Takhistov, P. T.; Miltz, J. Intelligent Packaging: Concepts and Applications. *Journal of Food Science* **2005,** *70* (1), R1-R10.
3. Podczeck, F.; Newton, J. M.; James, M. B. The influence of constant and changing relative humidity of the air on the autoadhesion force between pharmaceutical powder particles. *International Journal of Pharmaceutics* **1996,** *145* (1–2), 221-229.
4. Kidnay, A. J.; Parrish, W. R. *Fundamentals of natural gas processing*; CRC Press2006; Vol. 200.
5. Beyersmann, D.; Hartwig, A. The genetic toxicology of cobalt. *Toxicology and applied pharmacology* **1992,** *115* (1), 137-145.
6. Lauwerys, R.; Lison, D. Health risks associated with cobalt exposure — an overview. *Science of The Total Environment* **1994,** *150* (1–3), 1-6.
7. Stohs, S. J.; Bagchi, D. Oxidative mechanisms in the toxicity of metal ions. *Free Radical Biology and Medicine* **1995,** *18* (2), 321-336.

8. Hawkeye, M. M.; Brett, M. J. Optimized Colorimetric Photonic-Crystal Humidity Sensor Fabricated Using Glancing Angle Deposition. *Advanced Functional Materials* **2011,** *21* (19), 3652-3658.
9. Tian, E.; Wang, J.; Zheng, Y.; Song, Y.; Jiang, L.; Zhu, D. Colorful humidity sensitive photonic crystal hydrogel. *J.Mater.Chem.* **2008,** *18* (10), 1116-1122.
10. Xuan, R.; Wu, Q.; Yin, Y.; Ge, J. Magnetically assembled photonic crystal film for humidity sensing. *Journal of Materials Chemistry* **2011,** *21* (11), 3672-3676.
11. Luechinger, N. A.; Loher, S.; Athanassiou, E. K.; Grass, R. N.; Stark, W. J. Highly Sensitive Optical Detection of Humidity on Polymer/Metal Nanoparticle Hybrid Films. *Langmuir* **2007,** *23* (6), 3473-3477.
12. Lopes, P.; Saucier, C.; Teissedre, P.-L.; Glories, Y. Main routes of oxygen ingress through different closures into wine bottles. *Journal of agricultural and food chemistry* **2007,** *55* (13), 5167-5170.
13. Lopes, P.; Saucier, C.; Teissedre, P.-L.; Glories, Y. Impact of storage position on oxygen ingress through different closures into wine bottles. *Journal of agricultural and food chemistry* **2006,** *54* (18), 6741-6746.
14. Marmion, D. M. *Handbook of US colorants: foods, drugs, cosmetics, and medical devices*; John Wiley & Sons1991.
15. Saltmarsh, M.; Saltmarsh, M.; Barlow, S. *Essential guide to food additives*; Royal Society of Chemistry2013.
16. Gaunt, I. F.; Grasso, P.; Kiss, I. S.; Gangolli, S. D. Short-term toxicity study on Indigo Carmine in the pig. *Food and cosmetics toxicology* **1969,** *7* (0), 17-24.
17. Hooson, J.; Gaunt, I. F.; Kiss, I. S.; Grasso, P.; Butterworth, K. R. Long-term toxicity of indigo carmine in mice. *Food and cosmetics toxicology* **1975,** *13* (2), 167-176.
18. Fail, P. A.; Chapin, R. E.; Price, C. J.; Heindel, J. J. General, reproductive, developmental, and endocrine toxicity of boronated compounds. *Reproductive Toxicology* **1998,** *12* (1), 1-18.
19. Burdock, G. A. *Encyclopedia of food and color additives*; CRC Press1997; Vol. 3.
20. Villota, R.; Hawkes, J. G.; Cochrane, H. Food applications and the toxicological and nutritional implications of amorphous silicon dioxide. *Critical Reviews in Food Science & Nutrition* **1986,** *23* (4), 289-321.
21. Prado, A. G. S.; Bolzon, L. B.; Pedroso, C. P.; Moura, A. O.; Costa, L. L. Nb2O5 as efficient and recyclable photocatalyst for indigo carmine degradation. *Applied Catalysis B: Environmental* **2008,** *82* (3–4), 219-224.
22. Vautier, M.; Guillard, C.; Herrmann, J.-M. Photocatalytic Degradation of Dyes in Water: Case Study of Indigo and of Indigo Carmine. *Journal of Catalysis* **2001,** *201* (1), 46-59.
23. Sousa, M. M.; Miguel, C.; Rodrigues, I.; Parola, A. J.; Pina, F.; de Melo, J. S. S.; Melo, M. J. A photochemical study on the blue dye indigo: from solution to ancient Andean textiles. *Photochemical & Photobiological Sciences* **2008,** *7* (11), 1353-1359.
24. Zhang, C.; Khaliullin, R. Z.; Bovi, D.; Guidoni, L.; KÃ¼hne, T. D. Vibrational Signature of Water Molecules in Asymmetric Hydrogen Bonding Environments. *The Journal of Physical Chemistry Letters* **2013,** *4* (19), 3245-3250.
25. Ludvigsson, M.; Lindgren, J.; Tegenfeldt, J. FTIR study of water in cast Nafion films. *Electrochimica Acta* **2000,** *45* (14), 2267-2271.
26. Smith, B. C. *Infrared spectral interpretation: a systematic approach*; CRC press1998.

27. Vandeginste, B. G. M. t.; De Galan, L. Critical evaluation of curve fitting in infrared spectrometry. *Analytical Chemistry* **1975,** *47* (13), 2124-2132.
28. Jun, L.; Shuping, X.; Shiyang, G. FT-IR and Raman spectroscopic study of hydrated borates. *Spectrochimica Acta Part A: Molecular and Biomolecular Spectroscopy* **1995,** *51* (4), 519-532.
29. Momii, R. K.; Nachtrieb, N. H. Nuclear magnetic resonance study of borate- polyborate equilibria in aqueous solution. *Inorganic chemistry* **1967,** *6* (6), 1189-1192.
30. Zhou, Y.; Fang, C.; Fang, Y.; Zhu, F. Polyborates in aqueous borate solution: A Raman and DFT theory investigation. *Spectrochimica Acta Part A: Molecular and Biomolecular Spectroscopy* **2011,** *83* (1), 82-87.
31. Nyquist, R. A.; Kagel, R. O. *Handbook of infrared and raman spectra of inorganic compounds and organic salts: infrared spectra of inorganic compounds*; Academic press1972; Vol. 4.
32. Farmer, J. B. Metal Borates. In *Advances in Inorganic Chemistry*, Emeléus, H. J.; Sharpe, A. G., Eds.; Academic Press, 1982; Vol. Volume 25, pp 187-237.
33. Hua, D.; Hanxi, Y.; Xinping, A.; Chuansin, C. Hydrogen production from catalytic hydrolysis of sodium borohydride solution using nickel boride catalyst. *International Journal of Hydrogen Energy* **2003,** *28* (10), 1095-1100.
34. Marrero-Alfonso, E. Y.; Gray, J. R.; Davis, T. A.; Matthews, M. A. Minimizing water utilization in hydrolysis of sodium borohydride: the role of sodium metaborate hydrates. *International Journal of Hydrogen Energy* **2007,** *32* (18), 4723-4730.
35. Schlesinger, H. I.; Brown, H. C.; Finholt, A. E.; Gilbreath, J. R.; Hoekstra, H. R.; Hyde, E. K. Sodium Borohydride, Its Hydrolysis and its Use as a Reducing Agent and in the Generation of Hydrogen1. *Journal of the American Chemical Society* **1953,** *75* (1), 215-219.
36. BershteÄ-n, V. A.; Egorov, V. M. *Differential scanning calorimetry of polymers :physics, chemistry, analysis, technology*; Ellis Horwood: New York, 1994. p 253.
37. Grenier, G.; Westrum, E. F. The Heat Capacity and Thermodynamic Functions of Sodium Metaborate from 5 to 350Â°K. *Journal of the American Chemical Society* **1956,** *78* (24), 6226-6227.
38. Scovazzo, P.; Visser, A. E.; Davis Jr, J. H.; Rogers, R. D.; Koval, C. A.; DuBois, D. L.; Noble, R. D. Supported ionic liquid membranes and facilitated ionic liquid membranes. *ChemInform* **2002,** *33* (48), 240-240.

Table of Contents Figure: